



Published in final edited form as:

Cell Rep. 2017 November 28; 21(9): 2571–2584. doi:10.1016/j.celrep.2017.10.118.

## Quiescence Exit of Tert<sup>+</sup> Stem Cells by Wnt/ $\beta$ -Catenin Is Indispensable for Intestinal Regeneration

Han Na Suh<sup>1</sup>, Moon Jong Kim<sup>1</sup>, Youn-Sang Jung<sup>1</sup>, Esther M. Lien<sup>1</sup>, Sohee Jun<sup>1</sup>, and Jae-II Park<sup>1,2,3,4,\*</sup>

<sup>1</sup>Department of Experimental Radiation Oncology, Division of Radiation Oncology, The University of Texas MD Anderson Cancer Center, Houston, TX 77030, USA

<sup>2</sup>Graduate School of Biomedical Sciences, The University of Texas MD Anderson Cancer Center, Houston, TX 77030, USA

<sup>3</sup>Program in Genes and Development, The University of Texas MD Anderson Cancer Center, Houston, TX 77030, USA

### SUMMARY

Fine control of stem cell maintenance and activation is crucial for tissue homeostasis and regeneration. However, the mechanism of quiescence exit of Tert<sup>+</sup> intestinal stem cells (ISCs) remains unknown. Employing a Tert knock-in (Tert<sup>TCE/+</sup>) mouse model, we found that Tert<sup>+</sup> cells are long-term label-retaining self-renewing cells, which are partially distinguished from the previously identified +4 intestinal stem cells (ISCs). Tert<sup>+</sup> cells become mitotic upon irradiation (IR) injury. Conditional ablation of Tert<sup>+</sup> cells impairs IR-induced intestinal regeneration but not intestinal homeostasis. Upon IR injury, Wnt signaling is specifically activated in Tert<sup>+</sup> cells *via* the ROS-HIFs-transactivated Wnt2b signaling axis. Importantly, conditional knock-out of  $\beta$ -catenin/*Ctnnb1* in Tert<sup>+</sup> cells undermines IR-induced quiescence exit of Tert<sup>+</sup> cells, which subsequently impedes intestinal regeneration. Our results strongly suggest that Wnt signaling-induced activation of Tert<sup>+</sup> ISCs is indispensable for intestinal regeneration, which unveils the underlying mechanism of how Tert<sup>+</sup> stem cells undergo quiescence exit upon tissue injury.

### eTOC Blurbs

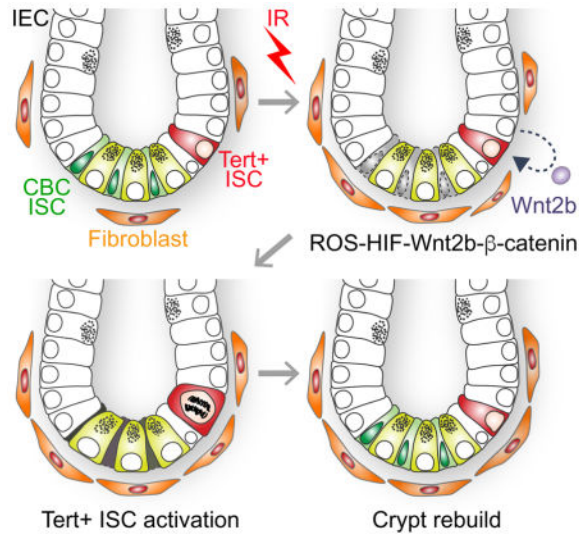
\*Correspondence: Jae-II Park, jaeil@mdanderson.org; Tel: 713-792-3659; Fax: 713-794-5369.

<sup>4</sup>Lead contact

#### AUTHOR CONTRIBUTIONS

H.N.S. and J.-I.P. conceived the experiments. H.N.S., M.J.K., Y.-S.J., E.M.L., S.J., and J.-I.P. performed the experiments. H.N.S. and J.-I.P. analyzed the data. H.N.S. and J.-I.P. wrote the manuscript.

**Publisher's Disclaimer:** This is a PDF file of an unedited manuscript that has been accepted for publication. As a service to our customers we are providing this early version of the manuscript. The manuscript will undergo copyediting, typesetting, and review of the resulting proof before it is published in its final citable form. Please note that during the production process errors may be discovered which could affect the content, and all legal disclaimers that apply to the journal pertain.



Suh et al. define *Tert*<sup>+</sup> cells as essential stem cells for intestinal regeneration, and unveil how *Tert*<sup>+</sup> intestinal stem cells escape from the quiescent state and repopulate into progenitor cells upon tissue injury.

### Keywords

intestinal stem cells; *Tert*; intestinal regeneration; Wnt/β-catenin; ROS-HIFs-Wnt2b

## INTRODUCTION

Stem cells (SCs) are consistently or conditionally activated for tissue homeostasis or regeneration (Barker, 2014). The fine tune of SC dynamics is governed by both cell intrinsic (Blanpain, et al., 2006; Lowell, et al., 2000), and extrinsic factors (Choi, et al., 2013; Lim, et al., 2013; Eisenhoffer, et al., 2012; Marinari, et al., 2012). The intestinal epithelium is composed of heterogeneous cell populations (absorptive enterocytes, secretive goblet cells, enteroendocrine cells, and Paneth cells), which originate from ISCs and are rapidly replenished from the crypts to the villi (Sancho, et al., 2003). Two distinct ISCs co-exist in the crypts (Barker, 2014). While the highly proliferative crypt base columnar (CBC) ISCs (*Lgr5*<sup>+</sup>) continuously generate intestinal epithelial cells (IECs) for tissue homeostasis (Snippert, et al., 2010), the relatively quiescent position 4 (+4) ISCs, located above the Paneth cells, are involved in intestinal regeneration (Yan, et al., 2012).

Several markers of quiescence ISC with distinct expression patterns have been identified. For example, +4 ISCs are co-localized with *Bmi1*-expression cells (Yan, et al., 2012; Sangiorgi and Capecchi, 2008), whereas *Bmi1* is broadly expressed in the crypt, including the *Lgr5*<sup>+</sup> cells (Itzkovitz, et al., 2012; Munoz, et al., 2012). In *Tert* transgenic mouse, *Tert*<sup>+</sup> cells are mainly located in the +5 to +8 position (Montgomery, et al., 2011). In addition, proliferative *Hopx*<sup>+</sup> cells are found at +4 after IR (Takeda, et al., 2011). Furthermore, quiescent labeled-retaining cells (LRCs) are thought to be the precursor of secretory cells expressing *Lgr5* (Buczacki, et al., 2013). Nonetheless, quiescent ISCs need to be further

validated given the various expression of *Lgr5* in the crypts. To overcome the current technical limitation in studying SCs, we recently generated a *Tert* knock-in mouse model (Jun, et al., 2016). *Tert*, a catalytic subunit of telomerase, is specifically expressed in self-renewing cells including SCs, germ cells, and cancer cells (Flores, et al., 2006). By utilizing *Tert* expression as a functional SC marker in our study, here, we explored the biology of *Tert* + SCs in tissue regeneration.

High-dose ionizing radiation induces the loss of crypt cells, resulting in radiation-induced gastrointestinal syndrome (RIGS) (Saha, et al., 2011). Owing to damaged stem cell population in the crypts, RIGS prevents the replenishment of intestinal epithelium and leads to several pathophysiological conditions including electrolyte imbalance, diarrhea, and weight loss (Zimmerer, et al., 2008). Recent therapeutic strategies for RIGS are transplantation of stromal cells (Saha, et al., 2011), treatment of R-spondin 1 (Bhanja, et al., 2009), or administration of macrophage-derived WNTs (Saha, et al., 2016), suggesting that Wnt/ $\beta$ -catenin signaling might be essential for tissue regeneration. Herein we dissected the mechanism of how ISCs are activated during intestinal regeneration.

## RESULTS

### Conditional repopulation of *Tert* + cells upon radiation injury

A *Tert* knock-in mouse (hereafter referred as *Tert*<sup>TCE/+</sup>) expresses tdTomato-CreERT2 (TCE) driven by the endogenous *Tert* promoter (Jun, et al., 2016) (Figure 1A). We first tested whether TCE protein conditionally induces Cre-loxP recombination. Tamoxifen (Tam) treatment induced the nuclear translocation of TCE protein and subsequent Cre-loxP recombination, represented by LacZ expression in 3TZ, Cre-loxP recombination reporter cells (Psarras, et al., 2004) (Figures 1B–1D). Employing *Tert*<sup>TCE/+</sup> mice, we found that *Tert* + cells resided at the +3~+4 position beyond CBC ISCs in the intestine, at a frequency of one *Tert*+ cell per  $120.5 \pm 26.50$  crypts (Figures 1E, S1A). To determine whether *Tert*+ cells are quiescent ISCs, we performed a label-retaining cell (LRC) assay by a single dose injection of 5-bromo-2'-deoxyuridine (BrdU) into *Tert*<sup>TCE/+</sup> mice (Hsu and Fuchs, 2012; Potten, et al., 2002). Three months after BrdU administration, we detected *Tert*-:BrdU+ (20.6%), *Tert*+:BrdU- (43%), and *Tert*+:BrdU+ (36.4%) in the crypts (Figures 1F and S1C), suggesting that some *Tert*+ cells are long-term LRCs. Consistently, BrdU incorporation assays (BrdU injection 0.5 hr prior to tissue collection) showed that *Tert*+ cells were not proliferative in the homeostatic intestine (Figure 1G). Next, we performed single cell gene expression analysis of *Tert*+ cells isolated from the intestinal crypt using fluorescence-activated cell sorting (FACS) (Figures 1H–1I, S1B). *Tert*+ cells exhibited the prominent enrichment for *Tert* and *Bmi1* expression (Figure 1J), however, immunofluorescent (IF) staining showed that not all *Tert*+ cells were *Bmi1*+ cells (Figures 1K and S1D). The progenitor cell markers (*Dll1*, *Krt19*, *Lrig1*, and *Alpi*) and non-homologous end joining DNA repair components (*Lig4*, *Xrcc5*, and *Xrcc4*) were also upregulated in *Tert*+ cells, whereas the expression of homologous recombination DNA repair-related genes (*Blm*, *Rpa1*, and *Rad51c*) did not show any difference between *Tert*+ and *Tert*- cells. Interestingly, *Tert*+ cells exhibited the high expression of cell cycle arrest-related genes (*p19*, *p107*, *p53*, *p130*, and *p21*), but no change in Wnt target gene expression

(*CD133*, *Axin2*, and *CD44*) compared to *Tert*<sup>-</sup> cells (Figure 1J). These results support that *Tert*<sup>+</sup> cells are long-term LRCs. Previously, it was reported that LRCs are secretory precursor cells (Buczacki, et al., 2013). To determine whether *Tert*<sup>+</sup> long-term LRCs share similar markers as secretory precursor cells, we performed IHC for detecting the Paneth cells or enteroendocrine cells. We found that *Tert*<sup>+</sup> cells are not co-localized with lysozyme<sup>+</sup> cells (the Paneth cell) (Figures 1L and S1E). Intriguingly, we located a few ChgA<sup>+</sup> cells in the crypts as *Tert*<sup>+</sup> cells (Figures 1M and S1F). These results were also confirmed by measuring the expression of *ChgA*, *ChgB*, and *Mmp7* in *Tert*<sup>+</sup> cells by quantitative reverse transcription polymerase chain reaction (qRT-PCR). Compared to *Tert*<sup>-</sup> cells, *Tert*<sup>+</sup> cells displayed an increase of enteroendocrine cell marker genes (*ChgA*, *ChgB*), whereas no enrichment of the Paneth cell marker gene (*Mmp7*) in *Tert*<sup>+</sup> cells was detected (Figure 1N). These results suggest that a small portion of *Tert*<sup>+</sup> cells includes enteroendocrine precursor cells but not Paneth cells, which partially supports the previous study (Buczacki, et al., 2013).

Given the specific expression of *Tert* in self-renewing cells (Hiyama and Hiyama, 2007), we hypothesized that *Tert*<sup>+</sup> cells are quiescent ISCs but conditionally repopulated upon tissue injury. To test this, mice were exposed to whole body irradiation (WBI; 10 Gy) for injury and monitored for intestinal regeneration. After ionizing radiation (IR), proliferating cells (transit-amplifying and CBC cells) were depleted mainly due to DNA damage as well as apoptosis (Figures 2A–2C, S2A–S2B). Interestingly, despite the massive depletion of IECs by IR, *Tert* mRNA was markedly upregulated in the crypt, implying the increase of *Tert*<sup>+</sup> cells and/or *Tert* mRNA during regeneration (Figure 2D). To clarify this, we determined whether IR induces proliferation of *Tert*<sup>+</sup> cells. While *Tert*<sup>+</sup> cells were non-proliferative (*Tert*<sup>+</sup>:*Ki67*<sup>-</sup>) during intestinal homeostasis, *Tert*<sup>+</sup> cells became proliferative after IR (Figures 2E–2H). The number of proliferative *Tert*<sup>+</sup> cells was increased until 2 dpi (days post injury) (more than four-fold) and restored at 4 dpi (Figure 2G). Single cell gene expression analysis of *Tert*<sup>+</sup> cells at 1 dpi showed an increase of *Cyclin D1* and *c-Myc* expression but decreased expression of *p21* (Figure 2I), supporting the notion that IR induces the proliferation of *Tert*<sup>+</sup> cells. Next, we asked whether mitotically activated *Tert*<sup>+</sup> cells generate IECs by employing lineage-tracing assay. *Tert*<sup>TCE/+</sup>:*R26eYFP* strain treated with Tam and IR exhibited repopulation of *Tert*<sup>+</sup> cells into IECs during regeneration (Figure 2J). Furthermore, given the co-existence of proliferative (*Lgr5*<sup>+</sup>) and quiescent (+ 4) ISCs in the intestinal crypts, we assessed the cell population kinetics between *Tert*<sup>+</sup> cells and *Lgr5*<sup>+</sup> ISCs during intestinal regeneration. Upon IR injury, most *Lgr5*<sup>+</sup> cells were depleted at 1 dpi and then recovered through 7 dpi. Conversely, *Tert*<sup>+</sup> cells were markedly increased until 2 dpi and returned to the basal level at 7 dpi (Figures 2K and S2C). Intriguingly, *Lgr5* mRNA expression in *Tert*<sup>+</sup> cells was significantly elevated at 1 dpi (Figure 2L) and the progeny of *Tert*<sup>+</sup> cells (YFP<sup>+</sup>) were found between the Paneth cells at the bottom of the crypt (Figure 2M). These results imply that *Tert*<sup>+</sup> cells might serve as a reservoir for *Lgr5*<sup>+</sup> cells during intestinal regeneration.

To be defined as SCs, SCs should repopulate into progenitor cells and self-renew. Having observed the repopulation of *Tert*<sup>+</sup> cells into IECs by injury (Figures 2J and 2M), we next asked whether *Tert*<sup>+</sup> cells are activated by successive injuries. We treated *Tert*<sup>TCE/+</sup> mice with sequential IR injuries (6 Gy, nonlethal dose but sufficient to induce intestinal injury) to

label the dividing cells along with the simultaneous injection of thymidine analogs (IdU for the first round of injury and CldU for the second round of injury) (Figures 2N–2P). We found that *Tert*<sup>+</sup> cells were labeled with both IdU and CldU after two consecutive regenerations (28 days later) (Figure 2P). Of note, due to the rapid replenishment of intestinal epithelium (3–5 days), only LRCs remain with IdU or CldU labeling. These results further suggest that *Tert*<sup>+</sup> cells are quiescent ISCs, which are conditionally repopulated into IECs during intestinal regeneration.

### Impaired intestinal regeneration by conditional ablation of *Tert*<sup>+</sup> cells

Having determined the quiescence exit of *Tert*<sup>+</sup> cells upon intestinal injury, we next asked whether *Tert*<sup>+</sup> cells are indispensable for intestinal regeneration. To address this, we generated a *Tert*<sup>TCE/+</sup>:*R26DTA* compound strain. Upon Tam administration, diphtheria toxin A (DTA) is specifically expressed in *Tert*<sup>+</sup> cells, which leads to their selective removal by cell death (about 70% removal of *Tert*<sup>+</sup> cells) (Figures 3A–3B, S3A–S3B). Before cell ablation experiments, we tested whether *de novo* generation of *Tert*<sup>+</sup> cells occurs.

*Tert*<sup>TCE/+</sup>:*R26DTA* mice were injected with Tam to deplete *Tert*<sup>+</sup> cells and assessed for *Tert*<sup>+</sup> cells using FACS. We found that *Tert*<sup>+</sup> cells were not generated up to 30 days after Tam administration, which excludes the potential *de novo* generation of *Tert*<sup>+</sup> cells in our experimental setting (Figures S4A–S4B). Next, we asked whether removal of *Tert*<sup>+</sup> cells impairs intestinal regeneration. Intriguingly, *Tert*<sup>TCE/+</sup>:*R26DTA* strain treated with Tam and IR (experimental group) showed the significant loss of intestinal epithelium integrity, decreased proliferation, and increased apoptosis in IECs of the crypts (Figures 3C–3G, S4C). It is noteworthy that other control groups without IR (*Tert*<sup>+/+</sup> and *Tert*<sup>TCE/+</sup>:*R26DTA* treated with Tam) displayed no defects in intestinal homeostasis (Figures S3C–S3J), indicating that *Tert*<sup>+</sup> cells are not essential for normal intestinal homeostasis. Additionally, upon *Tert*<sup>+</sup> cell ablation followed by IR, the intestinal epithelium showed abnormal lineage development of the Paneth cell, goblet cell, enterocyte, and enteroendocrine cell throughout the villi and crypts (Figures 3H–3K) as well as the increased mouse mortality (Figure S3K). These results suggest that *Tert*<sup>+</sup> cells are indispensable for intestinal regeneration.

### IR-activated Wnt/ $\beta$ -catenin signaling in *Tert*<sup>+</sup> cells via ROS-HIFs-Wnt2b

Next, we sought to dissect how tissue injury triggers the quiescence exit of *Tert*<sup>+</sup> cells for intestinal regeneration. To identify specific signaling pathway(s) involved in *Tert*<sup>+</sup> ISC activation, we performed gene expression analysis of several candidate signaling pathway target genes. We found that IR markedly upregulated Wnt target genes (*CD44*, *CD133*, and *Axin2*) in the crypts (Figure 4A), which was further confirmed by the increase of  $\beta$ -catenin reporter activity (X-gal staining of *Axin2-LacZ* mice),  $\beta$ -catenin protein, and  $\beta$ -catenin target gene expression (*CD44* and *Cyclin D1*) (Figures 4B–4E, S5A). These results suggest that IR activates Wnt/ $\beta$ -catenin signaling in the crypts, which implies the possible involvement of Wnt signaling in *Tert*<sup>+</sup> ISC activation.

Given the pivotal roles of Wnt ligands and agonists in the maintenance of intestinal integrity via  $\beta$ -catenin-mediated gene regulation (Farin, et al., 2012; Kim, et al., 2005), we hypothesized that IR-induced upregulation of Wnt ligands triggers target gene activation. To test this, we assessed the expression of nineteen Wnt ligands in the crypt ( $\pm$  IR). We found

that *Wnt2b*, *Wnt4*, *Wnt5a*, *Wnt6*, *Wnt7b*, and *Wnt9a* were upregulated by IR (Figures 4F, S5B). To further examine the localization and expression pattern of these Wnt ligands, we performed fluorescence in situ hybridization (FISH). Among the six Wnt ligands selected, *Wnt2b* expression was the most prominently upregulated in the intestinal epithelial cells of the crypts after IR (Figure 4H). We found that *Wnt4* is specifically expressed in the mesenchyme during intestinal homeostasis (non-IR treated) and in the epithelium during regeneration (IR-treated) (Figure S5E). *Wnt5a* was found expressed at the crypt-villus junction while *Wnt6* and *Wnt9a* were expressed in the crypt in both normal and regenerating intestine (Figures S5F, S5G, S5I). Lastly, *Wnt7b*-expressing cells were localized in the mesenchyme and were slightly upregulated by IR (Figure S5H). Upregulation of Wnt ligands from our semi-quantitative RT-PCR might be due to either transcriptional upregulation or increase of expressing cells. It is noteworthy that we observed an increased frequency of *Wnt5a*, *Wnt6*, or *Wnt9a*-expressing cells after IR, but not their transcriptional upregulation (Figures S5J–S5K). However, *Wnt2b* was the most significantly upregulated by IR at the transcriptional level and the increase of *Wnt2b*-expressing cells (Figure 4H). In the normal intestine, *Wnt2b* is expressed in the mesenchymal fibroblasts near the crypts (Valenta, et al., 2016) (Figures 4G–4H). To exclude the involvement of *Wnt2b* secreted from the mesenchymal cells, we isolated and cultured crypt IECs for the crypt organoid development and the subsequent IR treatment. FISH for *Wnt2b* showed that IR conditionally activated the *Wnt2b* expression in the mesenchymal cell-free crypt organoids (Figure 4I).

Next, we asked how IR upregulates *Wnt2b* in IECs. Given that IR increases reactive oxygen species (ROS) (Azzam, et al., 2012) and subsequently activates hypoxia-inducible factors (HIFs) (Moeller, et al., 2004), we tested whether the ROS-HIFs signaling axis mediates IR-induced *Wnt2b* upregulation. Indeed, IR increased ROS generation in the crypt and the normal IECs, represented by the increase of 8-Oxo-2'-deoxyguanosine (8-oxo-dG; an indirect marker of ROS) and 2',7'-dichlorodihydrofluorescein diacetate (H<sub>2</sub>DCFDA; a direct marker of intracellular ROS), respectively (Figures 4J–4K). Moreover, IR induced the nuclear translocation of HIF1 $\alpha$  in the crypt IECs and CCD841CoN IECs (Figures 4L–4M). Next, we determined whether IR activates HIFs through ROS. We found that the ROS inhibitor, N-acetyl cysteine (NAC), blocked the nuclear translocation of HIF1 $\alpha$  in IR-treated CCD841CoN IECs (Figure 4L). Of note, IR also induced the nuclear translocation of HIF2 $\alpha$  (Figure S5L). These data suggest that IR-induced HIF activation is mediated by ROS. Furthermore, we found that IR-induced *Wnt2b* upregulation was inhibited by NAC or chetomin (Chet, an inhibitor for HIFs) (Figure 4N), suggesting the potential involvement of ROS and HIFs in IR-induced *Wnt2b* upregulation.

Next, we tested whether HIFs directly transactivate *Wnt2b*. We identified multiple consensus hypoxia response elements (HRE; acgtg) in the conserved noncoding sequences (CNS) of both human and mouse *Wnt2b* promoter (Figure 4O), whereas other Wnt ligands (*Wnt4*, *Wnt5a*, *Wnt6*, *Wnt7b*, and *Wnt9a*) harbor fewer HREs (Figure S5J). These results imply that HIFs-transactivated *Wnt2b* might be evolutionarily conserved in mammals. Chromatin immunoprecipitation (ChIP) promoter scanning assays showed that HIF1 $\alpha$  conditionally occupied HREs at the *Wnt2b* promoter in mouse small intestine upon IR (Figure 4P). These results suggest that IR induces transactivation of *Wnt2b* via ROS-HIFs (Figure 4Q). Next, we tested whether IR-transactivated *Wnt2b* induces Wnt/ $\beta$ -catenin signaling activation in

IECs. In CCD841CoN IECs, treatment of either NAC or Chet suppressed IR-induced upregulation of *Axin2*, a  $\beta$ -catenin target gene (Figure 4R). We also found that ectopic *Wnt2b* expression is sufficient to activate Wnt/ $\beta$ -catenin signaling, as represented by *Axin2* upregulation in CCD841CoN IECs (Figure 4S). Conversely, depletion of endogenous *Wnt2b* decreased IR-induced *Axin2* upregulation (Figures 4T and S5C). These data suggest that IR activates Wnt/ $\beta$ -catenin signaling in IECs *via* the ROS-HIFs-*Wnt2b* signaling axis. Interestingly, it is noteworthy that IR-transactivated *Wnt2b* was only detected in *Tert*<sup>-</sup> IECs but not in *Tert*<sup>+</sup> cells in the crypts (Figure 4U). Nonetheless, we found that IR upregulated *Axin2* in *Tert*<sup>+</sup> cells (Figure 4V). To provide clearer evidence that *Wnt2b* is a critical downstream mediator of regeneration, we also performed knock-down assays for *Wnt2b* in the single cell-driven crypt organoids. Using lentivirus encoding shRNA against *mWnt2b*, we depleted the endogenous *Wnt2b* and treated the crypt organoids with IR. We found that *Wnt2b* knock-down inhibited the organoid growth under IR treated condition (Figures 4W and S5D). It is noteworthy that in the absence of IR treatment, *Wnt2b* shRNA did not affect the crypt organoid growth. This observation is consistent with the results that *Wnt2b* KO mice are viable without the defects in the intestinal homeostasis (Tsukiyama and Yamaguchi, 2012). These results suggest that IR activates Wnt/ $\beta$ -catenin signaling in *Tert*<sup>+</sup> cells *via* ROS-HIFs-*Wnt2b* signaling axis.

### Impaired intestinal regeneration by $\beta$ -catenin conditional knock-out in *Tert*<sup>+</sup> cells

Given the requirement of *Tert*<sup>+</sup> cells for intestinal regeneration (Figure 3) and IR-induced activation of Wnt/ $\beta$ -catenin signaling in *Tert*<sup>+</sup> cells (Figure 4V), we hypothesized that IR-activated Wnt/ $\beta$ -catenin signaling contributes to *Tert*<sup>+</sup> ISC activation and subsequent *Tert*<sup>+</sup> cell-driven intestinal regeneration. To test this, we genetically ablated  $\beta$ -catenin/*Ctnnb1* in *Tert*<sup>+</sup> cells by Tam administration into *Tert*<sup>TCE/+</sup>; *Ctnnb1*<sup>fl/fl</sup> mice (Figures 5A–5B). Isolated *Tert*<sup>+</sup> cells from the Tam-treated *Tert*<sup>TCE/+</sup>; *Ctnnb1*<sup>/</sup> strain displayed downregulation of  $\beta$ -catenin target genes (Figure 5C), indicating successful conditional knock-out (CKO) of  $\beta$ -catenin/*Ctnnb1*. Next, we examined the effects of  $\beta$ -catenin CKO in *Tert*<sup>+</sup> cells on intestinal regeneration. Indeed, Tam and IR-treated *Tert*<sup>TCE/+</sup>; *Ctnnb1*<sup>/</sup> mice showed impaired intestinal regeneration, represented by the loss of epithelium integrity, decreased proliferation, increased apoptosis, and abnormal distribution of IEC lineages (Figures 5D–5K). These results suggest that activation of Wnt/ $\beta$ -catenin in *Tert*<sup>+</sup> cells is crucial for intestinal regeneration.

Next, we questioned how Wnt/ $\beta$ -catenin engages in *Tert*<sup>+</sup> cell-mediated intestinal regeneration. Given IR-induced upregulation of cell proliferation-related and  $\beta$ -catenin target genes (*Ccnd1*, *c-Myc*, *Lgr5*, and *Axin2*) in *Tert*<sup>+</sup> cells (Figures 2I, 2L, 4V), we tested whether IR-induced Wnt/ $\beta$ -catenin activation is required for the quiescence exit of *Tert*<sup>+</sup> cells during intestinal regeneration. First, we assessed the effects of  $\beta$ -catenin CKO on the number of the intestinal *Tert*<sup>+</sup> cells. After  $\beta$ -catenin CKO, the number of *Tert*<sup>+</sup> cells was similar between *Tert*<sup>TCE/+</sup> and *Tert*<sup>TCE/+</sup>; *Ctnnb1*<sup>/</sup> in the homeostatic intestine (no IR) (Figures 5N, S6A). However, FACS analysis showed that  $\beta$ -catenin CKO in *Tert*<sup>+</sup> cells followed by IR reduced the number of proliferative *Tert*<sup>+</sup> cells (*Tert*<sup>+</sup>:Ki67+) (Figures 5O, S6B). Moreover, *Ccnd1* and *c-Myc* transcripts were significantly decreased in the small intestine of *Tert*<sup>TCE/+</sup>; *Ctnnb1*<sup>/</sup> mice upon IR, compared with those in *Tert*<sup>+/+</sup>; *Ctnnb1*<sup>+/+</sup>

mice (Figures 5L–5M). These results suggest that IR-activated Wnt/ $\beta$ -catenin signaling is required for the transition of Tert<sup>+</sup> cells from quiescent to proliferative status upon tissue injury.

## DISCUSSION

The quiescent ISCs have been identified as Bmi1 or *Hopx*-expressing cells as well as BrdU-retaining secretory precursors (Buczacki, et al., 2013; Takeda, et al., 2011; Sangiorgi and Capecchi, 2008). Interestingly, we observed that not all Tert<sup>+</sup> cells were colocalized with Bmi1<sup>+</sup> cells (see Figure 1K), indicating Tert<sup>+</sup> ISCs are somewhat distinguished from Bmi1<sup>+</sup> ISCs. Furthermore, unlike Buczacki's LRCs (Buczacki, et al., 2013), the markers of Tert<sup>+</sup> LRCs partially overlapped only with enteroendocrine cells but not Paneth cells (see Figures 1L–1N), which suggest the existence of additional quiescent ISCs. Although we here limited our scope to Tert<sup>+</sup> LRCs, it is probable that the different ISCs coordinately serve as multiple sources for repopulation into IECs during intestinal regeneration.

Importantly, given the contrasting kinetics of Lgr5<sup>+</sup> and Tert<sup>+</sup> cell populations (see Figure 2K), the marked induction of *Lgr5* expression in Tert<sup>+</sup> cells (see Figure 2L), and Tert<sup>+</sup> cell-driven progeny at the bottom of the crypt during regeneration (see Figure 2M), it is highly conceivable that the acute loss of Lgr5<sup>+</sup> cells by IR might be compensated by Tert<sup>+</sup> cells. Similarly, Hopx<sup>+</sup> and Bmi1<sup>+</sup> cells give rise to Lgr5<sup>+</sup> cells *ex vivo* (Takeda, et al., 2011; Tian, et al., 2011). This is consistent with the results that neither genetic ablation nor IR-induced removal of Lgr5<sup>+</sup> ISCs impairs intestinal integrity (Yan, et al., 2012); (Tian, et al., 2011). Therefore, it is highly likely that despite the removal of Lgr5<sup>+</sup> cells, Tert<sup>+</sup> cells serve as a reservoir for Lgr5<sup>+</sup> cells during regeneration. This is also supported by our results that the ablation of Tert<sup>+</sup> cells severely impairs intestinal regeneration (see Figures 3C–3K). Intriguingly, despite the crucial roles of Tert<sup>+</sup> cells in intestinal regeneration, the removal of Tert<sup>+</sup> cells did not affect intestinal homeostasis (see Figures S3C–S3J). Considering the cell plasticity in various regenerative tissues such as pancreas (Kopp, et al., 2016), intestine (Tetteh, et al., 2016; Asfaha, et al., 2015; van Es, et al., 2012), and lung (Tata, et al., 2013), our working model does not fully exclude the possibility that Tert<sup>+</sup> cells are generated from Tert<sup>–</sup> cells during intestinal regeneration, which should be carefully examined using the compound lineage-tracing experiments. Nonetheless, during intestinal homeostasis, no Tert<sup>+</sup> cells were generated (up to 30 days) after Tert<sup>+</sup> cell ablation (see Figures S4A–S4B), implying no *de novo* development of Tert<sup>+</sup> cells, at least, during intestinal homeostasis.

Employing our knock-in mouse model, we elucidate that Wnt/ $\beta$ -catenin signaling is required for the transition of Tert<sup>+</sup> cells from quiescence to mitotic activation. We observed that IR creates multiple DNA damage foci in most IECs in the crypts (see Figure 2B). IR directly induces DNA damage by random DNA breaks or indirectly through reactive oxygen species (ROS) generated by water hydrolysis (Azzam, et al., 2012). Although excessive ROS induces cell death, a moderate increase of ROS can regulate the activity of several downstream proteins including HIFs (Niecknig, et al., 2012; Gerald, et al., 2004). Indeed, IR increased ROS in the intestine followed by the direct recruitment of HIF-1 $\alpha$  to the *Wnt2b* promoter and subsequent *Wnt2b* transactivation (see Figures 4J, 4P). Furthermore, given the inhibitory effects of Chet on both HIF-1 $\alpha$  and HIF-2 $\alpha$  and the protective role of HIF-2 $\alpha$  in



the intestine (Taniguchi, et al., 2014; Xie, et al., 2014), HIF-2 $\alpha$  might also be involved in ROS-mediated *Wnt2b* transactivation.

We recently found that IR acutely activates Wnt/ $\beta$ -catenin signaling and transactivates *LIG4*, a core component of non-homologous end joining repair (Jun, et al., 2016). However, the detailed molecular mechanism of IR-activated Wnt/ $\beta$ -catenin signaling remained elusive. Our unbiased screening results of signaling pathways and Wnt ligands led us to select *Wnt2b* and the Wnt/ $\beta$ -catenin pathway as important mediators of Tert<sup>+</sup> cell activation during intestinal regeneration. *Wnt2b* functionally compensates for the loss of epithelial *Wnt3* in crypt organoid culture (Farin, et al., 2012; Goss, et al., 2009), indicating a role of *Wnt2b* in transducing canonical Wnt signaling. We found that IR markedly upregulates *Wnt2b* in IECs near +4 but not in Tert<sup>+</sup> cells (see Figures 4H, 4U), and *Wnt2b* knock-down inhibited organoid growth upon IR (see Figure 4W). Of note, *Wnt2b* was shown to activate canonical Wnt signaling ( $\beta$ -catenin-mediated) (Goss, et al., 2009). We found that IR activates Wnt/ $\beta$ -catenin signaling in Tert<sup>+</sup> cells (see Figure 4V), suggesting that IR-induced *Wnt2b* in IECs activates Wnt signaling in Tert<sup>+</sup> cells. Moreover, the results from  $\beta$ -catenin CKO in Tert<sup>+</sup> cells clearly demonstrated the requirement of Wnt/ $\beta$ -catenin signaling in Tert<sup>+</sup> cell activation and Tert<sup>+</sup> cell-driven intestinal regeneration (see Figures 5D–5K). Wnt signaling plays multiple roles in SC regulation including SC maintenance, activation, and differentiation (Lien and Fuchs, 2014). In our experimental condition, we found that  $\beta$ -catenin CKO in Tert<sup>+</sup> cells did not affect the number of Tert<sup>+</sup> cells but instead, suppressed the quiescence exit of Tert<sup>+</sup> cells (see Figures 5N–5O). This is also consistent with the reduced expression of cell proliferation-related genes in  $\beta$ -catenin CKO in Tert<sup>+</sup> cells (see Figures 5L–5M). Thus, our results strongly suggest that  $\beta$ -catenin is essential for the quiescence exit of Tert<sup>+</sup> cells during intestinal regeneration.

Despite the significance of Tert as a catalytic subunit of telomerase in self-renewing cells, the absence of accurate Tert reporter mouse models made it difficult to study Tert<sup>+</sup> cells. Unlike previous transgenic mice generated by pronuclear injection of *Tert* promoter-CreER DNA (Montgomery, et al., 2011), our model is a knock-in mouse strain established by blastocyst injection of targeted mouse embryonic stem cells. Given the limitation of transgenic mice mainly due to the random integration and uncontrolled copy number of the foreign DNA, gene targeting (knock-in) is more specific and reliable for representing physiological and pathological events of Tert<sup>+</sup> cells. Moreover, our *Tert* knock-in mouse model not only visualizes Tert<sup>+</sup> cells with tdTomato fluorescence, but also enables us to perform various cellular and genetic manipulation of Tert<sup>+</sup> cells using a CreERT2 cassette. Given that Tert is expressed in the self-renewing cells, future studies employing *Tert*<sup>TCE/+</sup> mice in different tissues (pancreas, liver, kidney, and hair follicle) may provide valuable insights into our understanding of tissue SCs. Furthermore, due to the reactivation of telomerase in human cancer, our *Tert* mouse models can also be used to isolate and characterize self-renewing tumor cells.

Together, our results define Tert<sup>+</sup> cells as essential ISCs for tissue regeneration and unveil how Tert<sup>+</sup> ISCs are conditionally activated from the quiescent state upon tissue injury (see Figure 6).

## EXPERIMENTAL PROCEDURES

### Animals

All mice were maintained in compliance with Institutional Animal Care and Use Committee (IACUC) guidelines of MD Anderson Cancer Center. Male and female mice (older than six weeks) were used for experiments. *Gt(ROSA)26Sor<sup>tm1(EYFP)Cos</sup>/J* (Jax strain 006148), *Gt(ROSA)26Sor<sup>tm1(DTA)Lky</sup>/J* (Jax strain 009669), *Cttnb1<sup>tm2Kem</sup>/K<sup>nmw</sup>J* (Jax strain 004152), and *Axin2<sup>LacZ</sup>* (Jax strain 009120) were purchased from Jackson Laboratory. Genotyping was performed following the Jackson Laboratory's protocol. Tam was dissolved in corn oil (Fisher) at a final concentration of 10 mg/ml for intraperitoneal (i.p.) administration (50 mg/kg). For intestine injury, mice were exposed to 10 Gy or 6 Gy (non-lethal dose for cell labeling) WBI, and tissues were collected at multiple time points.

### Label-retaining cell assay

*Tert<sup>TCE/+</sup>* mice were intraperitoneally administrated with 5-bromo-2'-deoxyuridine (BrdU, Sigma) (1 mg) at age 2 weeks. The tissue sample was collected at age 12 weeks and analyzed for *Tert*<sup>+</sup>:BrdU<sup>+</sup> cells in the crypt.

### FACS analysis

Intestinal crypts were isolated from *Tert<sup>TCE/+</sup>* mice. For single cell isolation, crypts were digested with Accumax (Stem cell technology 07921) for 20 min and collected through 70  $\mu$ m (BD 087712) and 40  $\mu$ m (BD 087711) cell strainers. Next, cells were suspended in phosphate-buffered saline (PBS) with 10% fetal bovine serum (FBS) and stained with SYTOX<sup>®</sup> Blue (Life Technologies S34857) to exclude dead cells. tdTomato fluorescence was detected by FACS (MoFlo<sup>®</sup> Astrios<sup>™</sup>, Beckman Coulter) and sorted into *Tert*<sup>+</sup> and *Tert*<sup>-</sup> cells among live cells based on the gate. Sorted *Tert*<sup>+</sup> and *Tert*<sup>-</sup> cells were analyzed for single cell gene expression profiling. To quantify the proliferation of *Tert*<sup>+</sup> cells, single cells isolated from crypt were fixed with 4% paraformaldehyde, blocked, incubated with a FITC-conjugated Ki67 antibody, and stained with DAPI. The population of *Tert*<sup>+</sup>:Ki67<sup>+</sup> was assessed by FACS (Gallios<sup>™</sup> 561, Beckman Coulter).

### Gene expression analysis

Isolated *Tert*<sup>+</sup> and *Tert*<sup>-</sup> cells (5 cells) were synthesized to complementary DNA (cDNA) using REPLI-g WTA Single Cell Kit (QIAGEN) and analyzed for single cell gene expression. For gene expression analysis, isolated crypts were processed for RNA extraction (QIAGEN RNeasy Mini Kit) and reverse transcription (iScript RT Supermix for RT-qPCR, Biorad). 18S ribosomal RNA (*18S rRNA*) was used as an endogenous control for normalization. qRT-PCR was performed using intron-spanning primers. Fold induction was quantified using the  $2^{-CT}$  method. For Figure 1J,  $CT$  values were displayed using Heatmap software (bar.utoronto.ca/). Primer sequences are listed in Supplementary Table 1.

### Dual-pulse labeling assay

*Tert<sup>TCE/+</sup>* mice were treated for the first tissue injury (6 Gy WBI) followed by 5-Iodo-2'-deoxyuridine (IdU, Sigma) (1 mg) i.p. injection. Two weeks later, *Tert<sup>TCE/+</sup>* mice were

treated for the second tissue injury (6 Gy WBI) followed by 5-Chloro-2'-deoxyuridine (CldU, Sigma) (1 mg) i.p. injection. After two weeks, the tissue was collected and analyzed for Tert<sup>+</sup>:IdU<sup>+</sup>:CldU<sup>+</sup> cells in the crypts.

### Fluorescence in situ hybridization

Fluorescence in situ hybridization (FISH) was performed according to the manufacturer's protocol (Invitrogen, FISH Tag™ RNA Green Kit, with Alexa Fluor® 488 dye). Probes were designed to be complementary to the coding sequences of *Wnt2b* (441 bp), *Wnt4* (421 bp), *Wnt5a* (437 bp), *Wnt6* (476 bp), *Wnt7b* (570 bp), and *Wnt9a* (401 bp). PCR products of Wnt ligands were inserted and transformed using TOPO®-TA Cloning (Invitrogen). Linearized plasmids (sense and antisense) were subjected to transcription, purification (amine-modified RNA), and labeling with the fluorescent dye (Alexa Fluor® 488). Intestine tissue slides were deparaffinized, processed for antigen retrieval (proteinase K, 10 µg/ml), and incubated with hybridization buffer (50% formamide, 5× SSC, 100 µg/ml fragmented salmon testes DNA, 50 µg/ml heparin, 0.1% Tween20). Tissue slides were then incubated with probe-fluorescent dye in hybridization buffer (1 µg/ml) at 55°C in a water bath for 20 h. The next day slides were washed with hybridization buffer, 50% hybridization buffer/PBS with 0.1% Tween 20 (PBT), and PBT. Slides were soaked with 70% glycerol/30% PBT and counterstained with 30 nM DAPI (Molecular Probes), and mounted with SlowFade® Gold Antifade Mountant (Thermo). A sense probe was used as a negative control.

### In silico promoter analysis

Conserved noncoding sequences (CNSs) were analyzed using the VISTA genome browser (<http://www-gsd.lidl.gov/vista/>). Briefly, the human and mouse *Wnt* ligands promoter was analyzed with default options (200-bp window, x-axis; 70% conservancy, y-axis) for potential hypoxia response elements (HREs; balloons). Promoter regions where peak values (y-axis) are above 50% were considered as potent evolutionarily conserved regulated elements.

### ChIP assays

Mouse intestines (non-treated and IR) were minced into small pieces, crosslinked with 1% formaldehyde for 15 min RT, and quenched by glycine (0.125 M). After washing with cold PBS, tissues were incubated with lysis buffer [0.5% NP-40, 25 mM HEPES, 150 mM KCl, 1.5 mM MgCl<sub>2</sub>, 10% glycerol and KOH (pH 7.5)] containing protease inhibitor for 15 min on ice. Cell lysates were centrifuged (5,000 r.p.m. for 5 min), and supernatants were discarded. Cell pellets were then subjected to sonication with ChIP-radioimmunoprecipitation assay (RIPA) lysis buffer (50 mM Tris, pH 8.0; 150 mM NaCl; 0.1% SDS, 0.5% deoxycholate, 1% NP-40 and 1 mM EDTA; 10 times, 30 s on/30 s off), using Bioruptor® Plus sonication device (Diagnode, NJ). After centrifugation (13,200 r.p.m. for 30 min), a supernatant was immunoprecipitated with antibody overnight at 4 °C and was pulled down using Dynabeads® Magnetic Beads (Thermo). Immunoprecipitates were further washed serially with ChIP-RIPA lysis buffer, high salt (50 mM Tris, pH 8.0; 500 mM NaCl; 0.1% SDS, 0.5% deoxycholate, 1% NP-40 and 1 mM EDTA), LiCl wash buffer (50 mM Tris, pH 8.0; 1 mM EDTA, 250 mM LiCl; 1% NP-40 and 0.5% deoxycholate) and Tris-EDTA buffer. Finally, immunoprecipitate crosslinking was reversed by incubation at 65 °C

overnight and treated with RNase A and proteinase K to extract DNA. ChIP amplicons (i–v) were detected via ChIP-PCR. Primer sequences for ChIP-PCR are available in Supplementary Table 1.

### Statistical analyses

The Student's *t*-test was used for comparisons of two samples. P values < 0.05 were considered significant. Error bars indicate s.e.m. The number of biological and experimental replicates is 3, unless otherwise mentioned in Figure Legends.

### Supplementary Material

Refer to Web version on PubMed Central for supplementary material.

### Acknowledgments

We thank Pierre D. McCrea, Junjie Chen, Seung-Hyo Lee, and Christopher L. Cervantes for helpful comments on the manuscript. This work was supported by the Cancer Prevention and Research Institute of Texas (RP140563), the National Institutes of Health (R01CA193297-01, P50CA098258), the Department of Defense (CA140572), the Duncan Family Institute for Cancer Prevention and Risk Assessment Grant (IRG-08-061-01), a Center for Stem Cell and Developmental Biology Transformative Grant (MD Anderson Cancer Center), an Institutional Research Grant (MD Anderson Cancer Center), a New Faculty Award (CA016672), and a Metastasis Research Center Grant (MD Anderson Cancer Center). The Genetically Engineered Mouse Facility was supported by the MD Anderson Cancer Center Support Grant (CA016672).

### References

- Asfaha S, Hayakawa Y, Muley A, Stokes S, Graham TA, Ericksen RE, Westphalen CB, von Burstin J, Mastracci TL, Worthley DL, et al. Krt19(+)/Lgr5(–) Cells Are Radioresistant Cancer-Initiating Stem Cells in the Colon and Intestine. *Cell Stem Cell*. 2015; 16:627–38. [PubMed: 26046762]
- Azzam EI, Jay-Gerin JP, Pain D. Ionizing radiation-induced metabolic oxidative stress and prolonged cell injury. *Cancer Lett*. 2012; 327:48–60. [PubMed: 22182453]
- Barker N. Adult intestinal stem cells: critical drivers of epithelial homeostasis and regeneration. *Nat Rev Mol Cell Biol*. 2014; 15:19–33. [PubMed: 24326621]
- Bhanja P, Saha S, Kabarriti R, Liu L, Roy-Chowdhury N, Roy-Chowdhury J, Sellers RS, Alfieri AA, Guha C. Protective role of R-spondin1, an intestinal stem cell growth factor, against radiation-induced gastrointestinal syndrome in mice. *PLoS One*. 2009; 4:e8014. [PubMed: 19956666]
- Blanpain C, Lowry WE, Pasolli HA, Fuchs E. Canonical notch signaling functions as a commitment switch in the epidermal lineage. *Genes Dev*. 2006; 20:3022–35. [PubMed: 17079689]
- Buczacki SJ, Zecchini HI, Nicholson AM, Russell R, Vermeulen L, Kemp R, Winton DJ. Intestinal label-retaining cells are secretory precursors expressing Lgr5. *Nature*. 2013; 495:65–9. [PubMed: 23446353]
- Choi YS, Zhang Y, Xu M, Yang Y, Ito M, Peng T, Cui Z, Nagy A, Hadjantonakis AK, Lang RA, et al. Distinct functions for Wnt/beta-catenin in hair follicle stem cell proliferation and survival and interfollicular epidermal homeostasis. *Cell Stem Cell*. 2013; 13:720–33. [PubMed: 24315444]
- Eisenhoffer GT, Loftus PD, Yoshigi M, Otsuna H, Chien CB, Morcos PA, Rosenblatt J. Crowding induces live cell extrusion to maintain homeostatic cell numbers in epithelia. *Nature*. 2012; 484:546–9. [PubMed: 22504183]
- Farin HF, Van Es JH, Clevers H. Redundant sources of Wnt regulate intestinal stem cells and promote formation of Paneth cells. *Gastroenterology*. 2012; 143:1518–1529. e7. [PubMed: 22922422]
- Flores I, Benetti R, Blasco MA. Telomerase regulation and stem cell behaviour. *Curr Opin Cell Biol*. 2006; 18:254–60. [PubMed: 16617011]

- Gerald D, Berra E, Frapart YM, Chan DA, Giaccia AJ, Mansuy D, Pouyssegur J, Yaniv M, Mechta-Grigoriou F. JunD reduces tumor angiogenesis by protecting cells from oxidative stress. *Cell*. 2004; 118:781–94. [PubMed: 15369676]
- Goss AM, Tian Y, Tsukiyama T, Cohen ED, Zhou D, Lu MM, Yamaguchi TP, Morrisey EE. Wnt2/2b and beta-catenin signaling are necessary and sufficient to specify lung progenitors in the foregut. *Dev Cell*. 2009; 17:290–8. [PubMed: 19686689]
- Hiyama E, Hiyama K. Telomere and telomerase in stem cells. *Br J Cancer*. 2007; 96:1020–4. [PubMed: 17353922]
- Hsu YC, Fuchs E. A family business: stem cell progeny join the niche to regulate homeostasis. *Nat Rev Mol Cell Biol*. 2012; 13:103–14. [PubMed: 22266760]
- Itzkovitz S, Lyubimova A, Blat IC, Maynard M, van Es J, Lees J, Jacks T, Clevers H, van Oudenaarden A. Single-molecule transcript counting of stem-cell markers in the mouse intestine. *Nat Cell Biol*. 2012; 14:106–14.
- Jun S, Jung YS, Suh HN, Wang W, Kim MJ, Oh YS, Lien EM, Shen X, Matsumoto Y, McCrea PD, et al. LIG4 mediates Wnt signalling-induced radioresistance. *Nat Commun*. 2016; 7:10994. [PubMed: 27009971]
- Kim KA, Kakitani M, Zhao J, Oshima T, Tang T, Binnerts M, Liu Y, Boyle B, Park E, Emtage P, et al. Mitogenic influence of human R-spondin1 on the intestinal epithelium. *Science*. 2005; 309:1256–9. [PubMed: 16109882]
- Kopp JL, Grompe M, Sander M. Stem cells versus plasticity in liver and pancreas regeneration. *Nat Cell Biol*. 2016; 18:238–45. [PubMed: 26911907]
- Lien WH, Fuchs E. Wnt some lose some: transcriptional governance of stem cells by Wnt/beta-catenin signaling. *Genes Dev*. 2014; 28:1517–32. [PubMed: 25030692]
- Lim X, Tan SH, Koh WL, Chau RM, Yan KS, Kuo CJ, van Amerongen R, Klein AM, Nusse R. Interfollicular epidermal stem cells self-renew via autocrine Wnt signaling. *Science*. 2013; 342:1226–30. [PubMed: 24311688]
- Lowell S, Jones P, Le Roux I, Dunne J, Watt FM. Stimulation of human epidermal differentiation by delta-notch signalling at the boundaries of stem-cell clusters. *Curr Biol*. 2000; 10:491–500. [PubMed: 10801437]
- Marinari E, Mehonic A, Curran S, Gale J, Duke T, Baum B. Live-cell delamination counterbalances epithelial growth to limit tissue overcrowding. *Nature*. 2012; 484:542–5. [PubMed: 22504180]
- Moeller BJ, Cao Y, Li CY, Dewhirst MW. Radiation activates HIF-1 to regulate vascular radiosensitivity in tumors: role of reoxygenation, free radicals, and stress granules. *Cancer Cell*. 2004; 5:429–41. [PubMed: 15144951]
- Montgomery RK, Carlone DL, Richmond CA, Farilla L, Kranendonk ME, Henderson DE, Baffour-Awuah NY, Ambruzs DM, Fogli LK, Algra S, et al. Mouse telomerase reverse transcriptase (mTert) expression marks slowly cycling intestinal stem cells. *Proc Natl Acad Sci U S A*. 2011; 108:179–84. [PubMed: 21173232]
- Munoz J, Stange DE, Schepers AG, van de Wetering M, Koo BK, Itzkovitz S, Volckmann R, Kung KS, Koster J, Radulescu S, et al. The Lgr5 intestinal stem cell signature: robust expression of proposed quiescent ‘+4’ cell markers. *EMBO J*. 2012; 31:3079–91. [PubMed: 22692129]
- Niecknig H, Tug S, Reyes BD, Kirsch M, Fandrey J, Berchner-Pfannschmidt U. Role of reactive oxygen species in the regulation of HIF-1 by prolyl hydroxylase 2 under mild hypoxia. *Free Radic Res*. 2012; 46:705–17. [PubMed: 22360728]
- Potten CS, Owen G, Booth D. Intestinal stem cells protect their genome by selective segregation of template DNA strands. *J Cell Sci*. 2002; 115:2381–8. [PubMed: 12006622]
- Psarras S, Karagianni N, Kellendonk C, Tronche F, Cosset FL, Stocking C, Schirmmacher V, Boehmer Hv H, Khazaie K. Gene transfer and genetic modification of embryonic stem cells by Cre- and Cre-PR-expressing MESV-based retroviral vectors. *J Gene Med*. 2004; 6:32–42. [PubMed: 14716675]
- Saha S, Aranda E, Hayakawa Y, Bhanja P, Atay S, Brodin NP, Li J, Asfaha S, Liu L, Tailor Y, et al. Macrophage-derived extracellular vesicle-packaged WNTs rescue intestinal stem cells and enhance survival after radiation injury. *Nat Commun*. 2016; 7:13096. [PubMed: 27734833]

- Saha S, Bhanja P, Kabarriti R, Liu L, Alfieri AA, Guha C. Bone marrow stromal cell transplantation mitigates radiation-induced gastrointestinal syndrome in mice. *PLoS One*. 2011; 6:e24072. [PubMed: 21935373]
- Sancho E, Batlle E, Clevers H. Live and let die in the intestinal epithelium. *Curr Opin Cell Biol*. 2003; 15:763–70. [PubMed: 14644203]
- Sangiorgi E, Capecchi MR. *Bmi1* is expressed in vivo in intestinal stem cells. *Nat Genet*. 2008; 40:915–20. [PubMed: 18536716]
- Snippert HJ, van der Flier LG, Sato T, van Es JH, van den Born M, Kroon-Veenboer C, Barker N, Klein AM, van Rheenen J, Simons BD, et al. Intestinal crypt homeostasis results from neutral competition between symmetrically dividing *Lgr5* stem cells. *Cell*. 2010; 143:134–44. [PubMed: 20887898]
- Takeda N, Jain R, LeBoeuf MR, Wang Q, Lu MM, Epstein JA. Interconversion between intestinal stem cell populations in distinct niches. *Science*. 2011; 334:1420–4. [PubMed: 22075725]
- Taniguchi CM, Miao YR, Diep AN, Wu C, Rankin EB, Atwood TF, Xing L, Giaccia AJ. PHD inhibition mitigates and protects against radiation-induced gastrointestinal toxicity via HIF2. *Sci Transl Med*. 2014; 6:236ra64.
- Tata PR, Mou H, Pardo-Saganta A, Zhao R, Prabhu M, Law BM, Vinarsky V, Cho JL, Breton S, Sahay A, et al. Dedifferentiation of committed epithelial cells into stem cells in vivo. *Nature*. 2013; 503:218–23. [PubMed: 24196716]
- Tetteh PW, Basak O, Farin HF, Wiebrands K, Kretzschmar K, Begthel H, van den Born M, Korving J, de Sauvage F, van Es JH, et al. Replacement of Lost *Lgr5*-Positive Stem Cells through Plasticity of Their Enterocyte-Lineage Daughters. *Cell Stem Cell*. 2016; 18:203–13. [PubMed: 26831517]
- Tian H, Biehs B, Warming S, Leong KG, Rangell L, Klein OD, de Sauvage FJ. A reserve stem cell population in small intestine renders *Lgr5*-positive cells dispensable. *Nature*. 2011; 478:255–9. [PubMed: 21927002]
- Tsukiyama T, Yamaguchi TP. Mice lacking *Wnt2b* are viable and display a postnatal olfactory bulb phenotype. *Neurosci Lett*. 2012; 512:48–52. [PubMed: 22326927]
- Valenta T, Degirmenci B, Moor AE, Herr P, Zimmerli D, Moor MB, Hausmann G, Cantu C, Aguet M, Basler K. Wnt Ligands Secreted by Subepithelial Mesenchymal Cells Are Essential for the Survival of Intestinal Stem Cells and Gut Homeostasis. *Cell Rep*. 2016; 15:911–8. [PubMed: 27117411]
- van Es JH, Sato T, van de Wetering M, Lyubimova A, Nee AN, Gregorieff A, Sasaki N, Zeinstra L, van den Born M, Korving J, et al. *Dll1*+ secretory progenitor cells revert to stem cells upon crypt damage. *Nat Cell Biol*. 2012; 14:1099–104. [PubMed: 23000963]
- Xie L, Xue X, Taylor M, Ramakrishnan SK, Nagaoka K, Hao C, Gonzalez FJ, Shah YM. Hypoxia-inducible factor/MAZ-dependent induction of caveolin-1 regulates colon permeability through suppression of occludin, leading to hypoxia-induced inflammation. *Mol Cell Biol*. 2014; 34:3013–23. [PubMed: 24891620]
- Yan KS, Chia LA, Li X, Ootani A, Su J, Lee JY, Su N, Luo Y, Heilshorn SC, Amieva MR, et al. The intestinal stem cell markers *Bmi1* and *Lgr5* identify two functionally distinct populations. *Proc Natl Acad Sci U S A*. 2012; 109:466–71. [PubMed: 22190486]
- Zimmerer T, Bocker U, Wenz F, Singer MV. Medical prevention and treatment of acute and chronic radiation induced enteritis--is there any proven therapy? a short review. *Z Gastroenterol*. 2008; 46:441–8. [PubMed: 18461520]

**Highlights**

- Tert+ cells are quiescent but conditionally repopulated upon tissue injury.
- Tert+ cells are indispensable for intestinal regeneration.
- ROS-HIFs-transactivated *Wnt2b* hyperactivates Wnt signaling in Tert+ cells.
- $\beta$ -catenin induces quiescence exit of Tert+ cells.

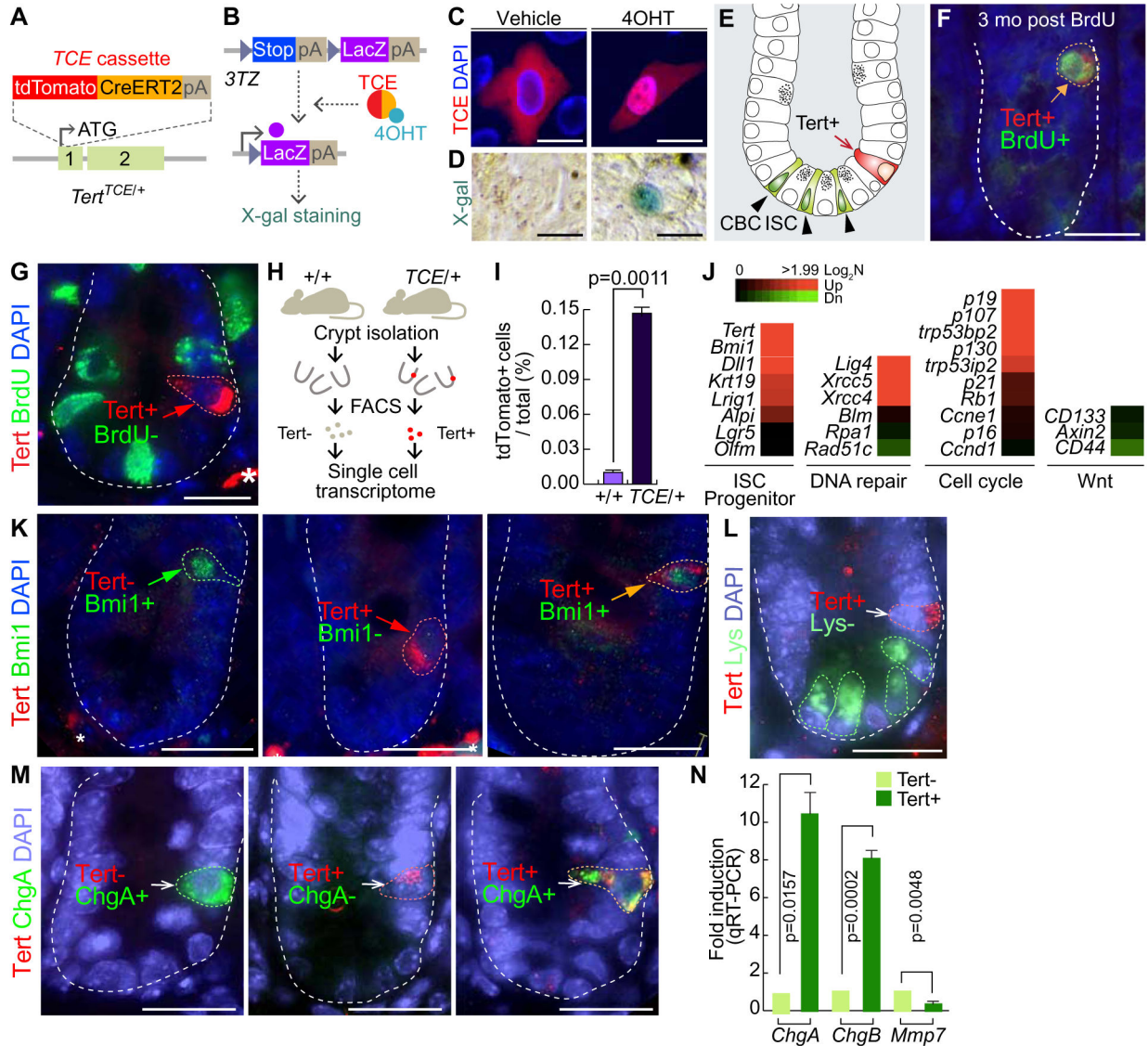


**Figure 1. Characterization of *Tert*<sup>+</sup> cells in the intestine**

(A) Generation of the *Tert*<sup>TCE/+</sup> knock-in mouse model by gene targeting. tdTomato-CreERT2 (TCE) cassette was inserted in frame into the *Tert* allele.

(B) Conditional activation of TCE by 4-hydroxytamoxifen (4OHT). 3TZ cells were transfected with a TCE-expressing plasmid. 4OHT-activated TCE induces Cre-loxP recombination, resulting in expression of LacZ, detected by β-galactosidase (X-gal) staining. (C) Nuclear translocation of TCE by 4-OHT. HeLa cells were transfected with TCE plasmid and treated with 4OHT (100 μM for 24 hr). Scale bars=20μm.

(D) TCE-induced Cre-LoxP recombination by 4-OHT. 3TZ cells were transfected with TCE plasmid, treated with 4OHT (100 μM for 36 hr), and visualized by β-galactosidase (X-gal) staining. Scale bars=20μm.



**(E)** Illustration of ISC and Tert+ cells in the small intestine. Tert+ cells are located at position 4 (+4) (arrow), while the crypt base columnar (CBC) ISCs are located at the bottom of crypts (arrowheads).

**(F)** Label-retaining cell assay. *Tert*<sup>TCE/+</sup> mice (2 wk of age) were injected with BrdU and tissues collected at 3 mo of age. Tert+:BrdU+ cell is indicated by an arrow. Scale bars=20µm.

**(G)** 5-Bromo-2-deoxyuridine (BrdU) incorporation assay. Briefly, *Tert*<sup>TCE/+</sup> mice were injected with BrdU (1 mg in PBS) 30 min before tissue collection and the small intestine was subjected to IF staining. Tert+:BrdU- cells are indicated by an arrow. Asterisk: non-specific signal. Scale bars=20µm.

**(H-I)** Detection and isolation of Tert+ cells using fluorescence-activated cell sorting (FACS).

**(J)** Single cell gene expression profiling of Tert+ cells compared to Tert- cells.

**(K)** Tert+ cells partially overlap with Bmi1+ cells in the small intestine.

**(L)** Tert+ cells do not overlap with lysozyme+ cells (Paneth cell) in the small intestine.

**(M)** Tert+ cells partially overlap with ChgA+ cells (enteroendocrine cell) in the small intestine. IHC of Tert- :Bmi1+, Tert+:Bmi1-, Tert+:Bmi1+, Tert+:Lysozyme-, Tert- :ChgA+, Tert+:ChgA-, Tert+:ChgA+ cells from the *Tert*<sup>TCE/+</sup> mice. Scale bars=20µm.

**(N)** Expression of *ChgA*, *ChgB*, and *Mmp7* in Tert+ cells. Tert+ cells were isolated from *Tert*<sup>TCE/+</sup> mice and markers for Paneth and enteroendocrine cells were assessed by qRT-PCR. Tert- cells were used as the control sample. Error bars indicate s.e.m.

The representative images are shown; N 3.

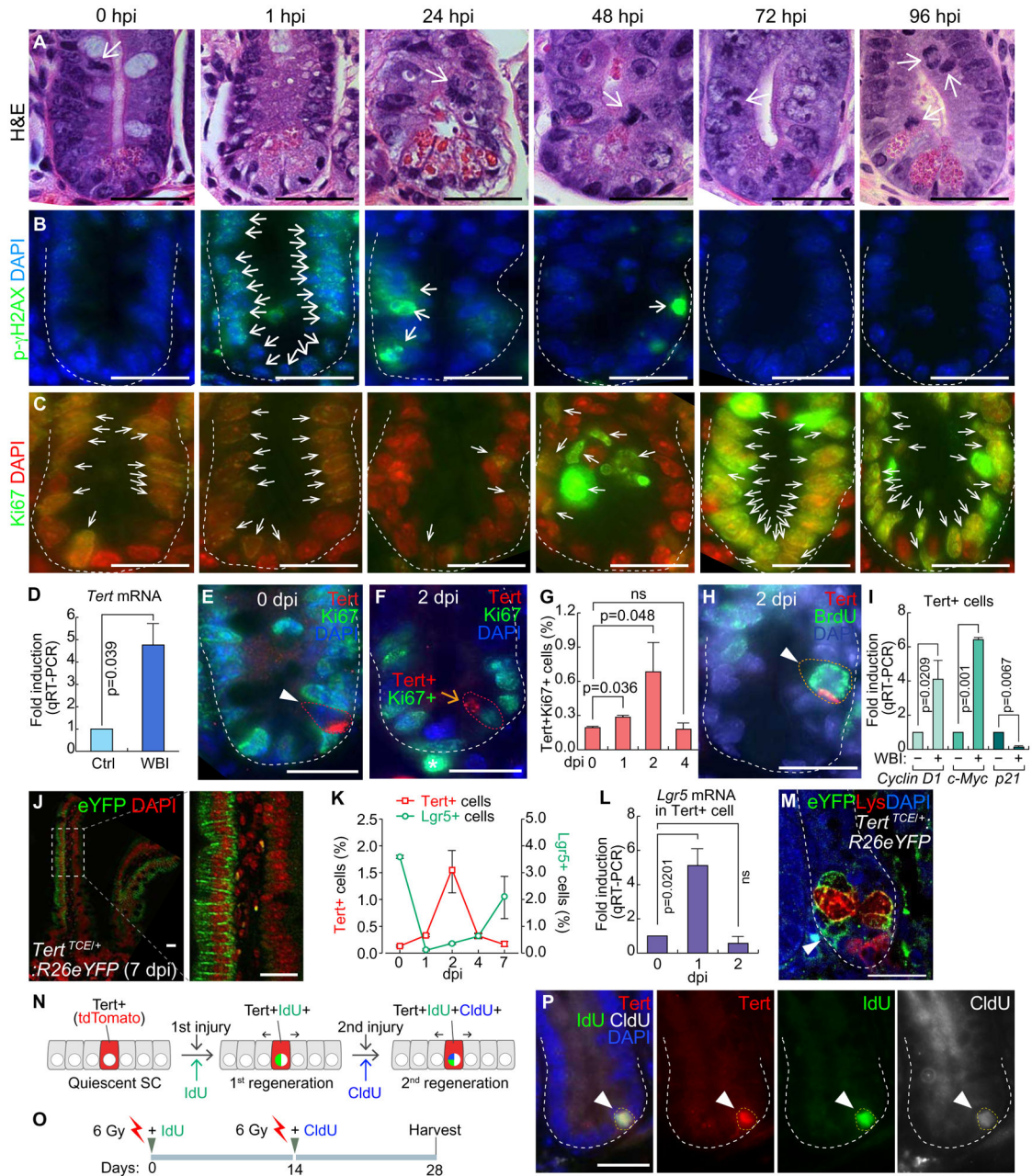


**Figure 2. Quiescence exit of *Tert*<sup>+</sup> cells upon radiation injury**

(A–C) Regeneration of intestinal crypt upon IR injury. Mice (5 wk) were treated with whole body irradiation (WBI; 10 Gy; a single dosage). H&E staining (A); DNA damage foci (phospho-gamma histone H2AX) (B); proliferation (Ki67) (C). Hour post injury (hpi); scale bars=20µm.

(D) *Tert* mRNA upregulation in the crypts after WBI (10 Gy). qRT-PCR of intestinal crypts at 24 hpi.

(E) Quiescence of *Tert*<sup>+</sup> cells during intestinal homeostasis. *Tert*<sup>+</sup>:Ki67<sup>-</sup> cells (arrowhead) of *Tert*<sup>TCE/+</sup> mice. Day post injury (dpi); scale bars=20µm.

**(F)** Activation of Tert+ cells during regeneration (10 Gy, 2 dpi). Tert+:Ki67+ cells (arrow) of *Tert*<sup>TCE/+</sup> mice. Scale bar=20µm.

**(G)** Quiescence exit of Tert+ cells by WBI. *Tert*<sup>TCE/+</sup> mice treated with WBI (10 Gy) were collected (0, 1, 2, and 4 dpi) for assessing Tert+:Ki67+ cells using FACS.

**(H)** Mitotic activation of Tert+ cells by WBI. *Tert*<sup>TCE/+</sup> mice were treated with WBI (10 Gy). At 2 dpi, BrdU (1mg/ml, i.p.) was administrated 30 min before tissue collection and the small intestine was subjected to IF staining. Tert+:BrdU+ cells (arrowhead). Scale bars=20µm.

**(I)** Expression of cell cycle-related genes in Tert+ cells. *Tert*<sup>TCE/+</sup> mice were treated with WBI (10 Gy, 24 hpi) and subjected to Tert+ cell isolation from intestinal crypts using FACS and qRT-PCR for *Cyclin D1*, *c-Myc*, and *p21* expression.

**(J)** Lineage-tracing of Tert+ cells. *Tert*<sup>TCE/+</sup>:*R26eYFP* mice were treated with 4OHT and WBI (10 Gy). At 7 dpi, cryosectioned, small intestine samples were analyzed for YFP expression.

**(K)** Comparative analysis of Tert+ and Lgr5+ cell populations after WBI (10 Gy). FACS analysis of Tert+ cells (tdTomato) from *Tert*<sup>TCE/+</sup> and Lgr5+ cells (GFP) from *Lgr5*<sup>EGFP-IRES-creERT2</sup> mouse models.

**(L)** Expression of *Lgr5* in Tert+ cells. *Tert*<sup>TCE/+</sup> mice were treated with WBI (10 Gy; 0, 1, 2 dpi) and subjected to Tert+ cell isolation from intestinal crypts using FACS and qRT-PCR for *Lgr5* expression.

**(M)** Lineage-tracing of Tert+ cells. *Tert*<sup>TCE/+</sup>:*R26eYFP* mice were treated with 4OHT and WBI (10 Gy). At 7 dpi, YFP+ cells (arrowhead) were found at the bottom of the crypt in between Paneth cells (lysozyme+ cells).

**(N–P)** Sequential injury-induced Tert+ cell activation. Illustration of Tert+ cell activation by consecutive tissue injuries **(N)**. Scheme of mouse treatment **(O)**. Of note, instead of a lethal dose (10 Gy), a sub-lethal dose WBI (6 Gy) was used, with IdU and CldU. Tert+:IdU+:CldU+ cells were visualized (28 dpi; arrowhead) **(P)**.

The representative images are shown; N 3; error bars indicate s.e.m.; ns: non-significant (P 0.05).

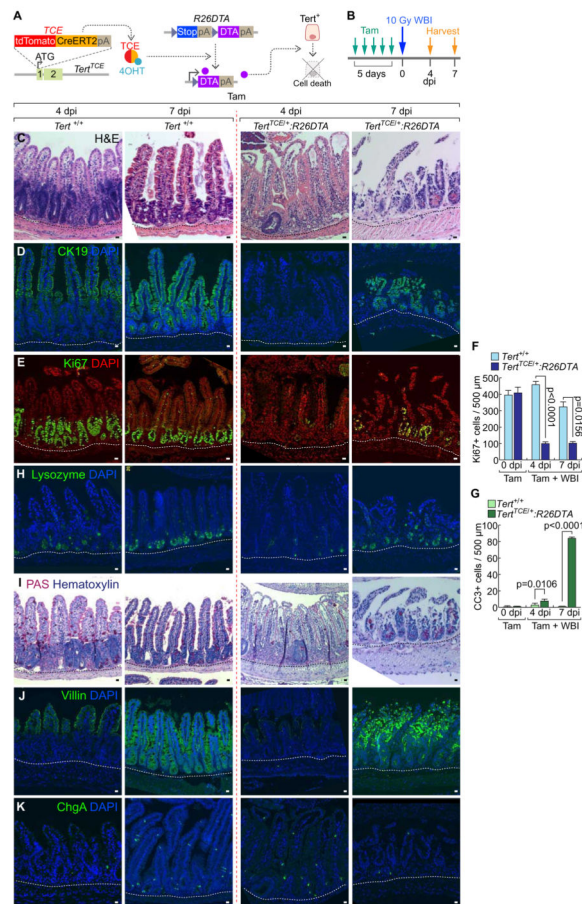


### Figure 3. Impaired intestinal regeneration by conditional ablation of *Tert*<sup>+</sup> cells

(A) Illustration of conditional ablation of *Tert*<sup>+</sup> cells (*Tert*<sup>TCE/+</sup>:*R26DTA*). 4OHT treatment activates TCE, which leads to the expression of diphtheria toxin A (DTA) for *Tert*<sup>+</sup> cell ablation.

(B) Scheme of mouse treatment.

(C–K) Impairment of intestinal regeneration by *Tert*<sup>+</sup> cell ablation. H&E staining (C); cytokeratin 19 (CK19) (D); Ki67 (E); lysozyme (Paneth cell, H); PAS (goblet cell, I); villin (enterocyte, J); chromogranin A (ChgA; enteroendocrine cell, K). Of note, Tam-treated *Tert*<sup>TCE/+</sup>:*R26DTA* did not affect intestinal homeostasis (Figures S3B–S3I). Quantification of the number of Ki67<sup>+</sup> cells (F) and CC3<sup>+</sup> cells (G) per 500 μm region of crypts. Scale bars=20 μm; dot lines indicate the basal membranes below crypts.

The representative images are shown; N = 3.

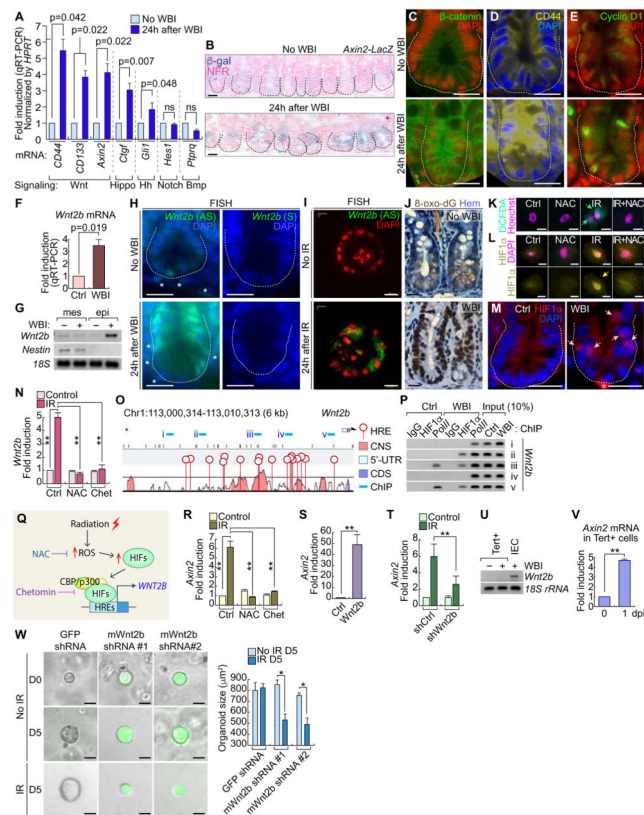


#### Figure 4. IR-activated Wnt/ $\beta$ -catenin signaling in the crypts and Tert<sup>+</sup> cells

(A) IR-induced upregulation of Wnt signaling target genes (*CD44*, *CD133*, and *Axin2*).

qRT-PCR of intestinal crypts isolated from mice treated with WBI (10 Gy, 24 hpi).

(B–E) IR-induced Wnt/ $\beta$ -catenin signaling activation in intestinal crypt. WBI (10 Gy, 24 hpi). X-gal staining in *Axin2-LacZ* intestine (B); IHC for  $\beta$ -catenin (C); CD44 (D) Cyclin D1 (E). Scale bars=20 $\mu$ m.

(F) *Wnt2b* upregulation in crypts by WBI (10 Gy, 24 hpi). qRT-PCR.

(G) IR-induced *Wnt2* upregulation in the crypt epithelial cells. WBI (10 Gy, 24 hpi). Semi-quantitative (sq) RT-PCR.

(H) *Wnt2b* upregulation in crypts by WBI (10 Gy). Fluorescence in situ hybridization (FISH). AS: antisense; S: sense probes; scale bars=20 $\mu$ m; asterisks: Wnt2b<sup>+</sup> mesenchymal cells.

(I) *Wnt2* upregulation in crypt organoids by IR (8 Gy). Fluorescence in situ hybridization (FISH). AS: antisense; scale bars=20 $\mu$ m.

(J) IR-induced ROS generation in the crypt. IHC for 8-Oxo-2'-deoxyguanosine (8-oxo-dG). Scale bars=20 $\mu$ m.

(K) IR-induced ROS generation in CCD841CoN IEC cells (10 Gy, 0.5 hr). DCFDA staining.

(L) IR-induced HIF1 $\alpha$  activation via ROS in CCD841CoN. Cells were pre-treated with N-acetyl-L-cysteine (NAC, 1 mM) for 4 hr and exposed to IR (10 Gy). After 24 hr, cells were analyzed by IF staining for HIF1 $\alpha$ . Scale bars=20 $\mu$ m.

(M) IR-induced HIF1 $\alpha$  nuclear translocation in the crypt. WBI (10 Gy, 24 hpi); scale bars=20 $\mu$ m; asterisks: non-specific signal.

- (N)** IR-induced *Wnt2* transactivation *via* ROS-HIFs in CCD841CoN. Cells were pre-treated with NAC or chetomin (100 nM) for 4 hr. After IR exposure (10 Gy, 24 hr), cells were analyzed for qRT-PCR.
- (O)** *Wnt2b* promoter analysis for hypoxia response element (HRE). Conserved non-coding sequence (CNS); coding sequence (CDS); 5 ChIP amplicons (i–v).
- (P)** IR-induced recruitment of HIF1 $\alpha$  to *Wnt2b* promoter in the small intestine. Small intestine samples from mice ( $\pm$ WBI [10 Gy], 24 hr) were analyzed for ChIP assays. RNA polymerase II (*Pol*II) served as a positive control for transcriptional activation.
- (Q)** Illustration of radiation-induced Wnt/ $\beta$ -catenin signaling activation *via* ROS-HIFs-*Wnt2b*.
- (R)** Inhibition of IR-induced *Axin2* by NAC or chetomin. CCD841CoN cells were pre-treated with NAC or chetomin, treated with IR (10 Gy, 24 hr), and analyzed by qRT-PCR.
- (S)** *Wnt2b*-activated  $\beta$ -catenin signaling activation. CCD841CoN cells were transfected with *Wnt2b* expression plasmids. 24 hr after transfection, cells were analyzed by qRT-PCR for *Axin2*.
- (T)** *Wnt2b* mediates IR-induced Wnt/ $\beta$ -catenin signaling activation. CCD841CoN cells were stably transduced with lentiviruses encoding shRNAs against *Wnt2b*, and then treated with IR (10 Gy, 24 hr) followed by qRT-PCR analysis of *Axin2*.
- (U)** No expression of *Wnt2b* in *Tert*<sup>+</sup> cells. Semi-quantitative (sq)RT-PCR. IECs isolated from the crypts served as positive control.
- (V)** *Axin2* upregulation by IR in *Tert*<sup>+</sup> cells. qRT-PCR of *Axin2* in *Tert*<sup>+</sup> cells isolated from *Tert*<sup>TCE/+</sup> mice treated with WBI (10 Gy; 1 dpi). The representative images are shown; N 3; error bars indicate s.e.m. double asterisks (\*\*)=P<0.05.
- (W)** Knock-down of *Wnt2b* in crypt single cell organoids. Lentiviruses expressing mouse *Wnt2b* shRNAs (clone #1~#2) inhibited organoid growth after IR (4 Gy). GFP shRNA was used as a negative control. Scale bars=20 $\mu$ m; asterisks (\*)=P<0.05.

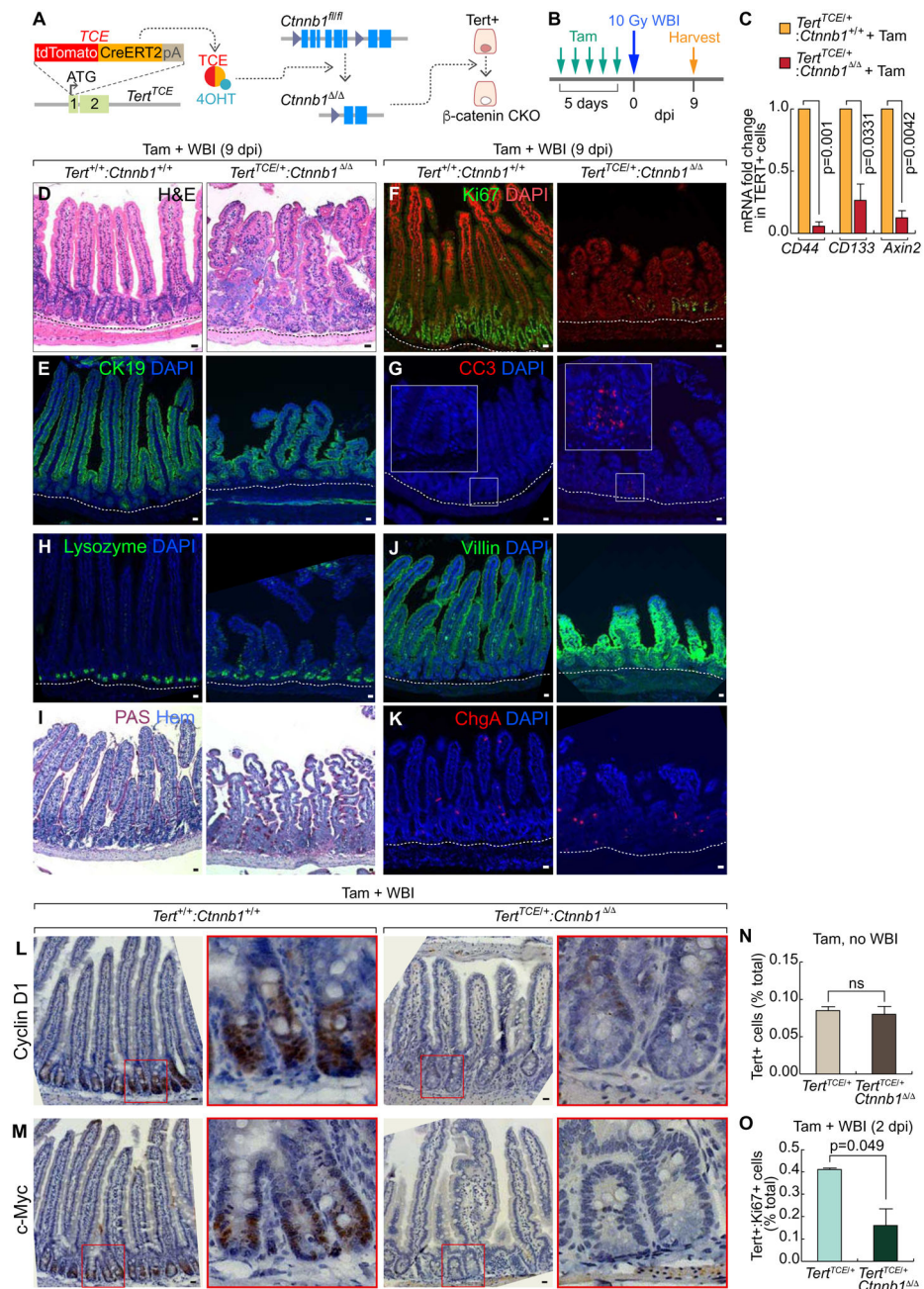


**Figure 5. Impaired intestinal regeneration by  $\beta$ -catenin conditional knockout in  $Tert^+$  cells**  
**(A)** Illustration of  $\beta$ -catenin/*Ctnnb1* conditional knock-out (CKO) in  $Tert^+$  cells ( $TERT^{TCE/+};Ctnnb1^{fl/fl}$ ).  
**(B)** Scheme of mouse treatment.  
**(C)**  $\beta$ -catenin CKO-induced downregulation of Wnt/ $\beta$ -catenin target gene expression in  $Tert^+$  cells. qRT-PCR of  $Tert^+$  cells for *CD44*, *CD133*, and *Axin2* expression from  $Tert^{TCE/+}$  (control) and  $Tert^{TCE/+};Ctnnb1^{-/-}$  (experimental group) treated with tamoxifen.

**(D–K)** IHC of impaired intestinal regeneration by  $\beta$ -catenin CKO in *Tert*<sup>+</sup> cells. H&E staining (**D**); CK19 (**E**); Ki67 (**F**); CC3 (**G**); lysozyme (**H**); PAS (**I**); villin (**J**); ChgA (**K**). Scale bars=20 $\mu$ m.

**(L–M)** Cell cycle-related gene expression in *Tert*<sup>+/+</sup>;*Ctnnb1*<sup>+/+</sup> and *Tert*<sup>TCE/+</sup>;*Ctnnb1*<sup>/</sup> (10 Gy, 7 dpi). Cyclin D1 (**L**); c-Myc (**M**). Scale bars=20 $\mu$ m. Cyclin D1 and c-Myc were significantly downregulated by  $\beta$ -catenin CKO in *Tert*<sup>+</sup> cells and WBI.

**(N)** No loss of *Tert*<sup>+</sup> cells by  $\beta$ -catenin CKO during intestinal homeostasis. Population analysis of *Tert*<sup>+</sup> cells after Tam treatment in *Tert*<sup>TCE/+</sup> and *Tert*<sup>TCE/+</sup>;*Ctnnb1*<sup>/</sup>, using FACS. ns: non-significant ( $p > 0.05$ ).

**(O)** Reduced proliferation of *Tert*<sup>+</sup> cells during intestinal regeneration by  $\beta$ -catenin CKO. Quantification of *Tert*<sup>+</sup>:Ki67<sup>+</sup> cells of Tam and IR (10 Gy; 2 dpi)-treated *Tert*<sup>TCE/+</sup> and *Tert*<sup>TCE/+</sup>;*Ctnnb1*<sup>/</sup> mice, using FACS.

The representative images are shown; N 3; error bars indicate s.e.m.



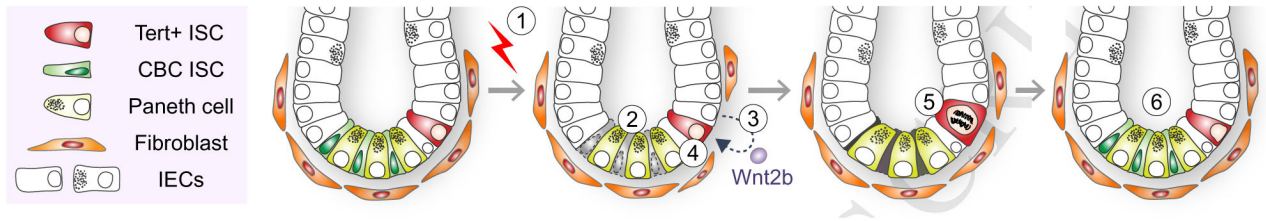


**Figure 6. Illustration of working model**

IR induces the death of mitotic cells (TA and CBC ISCs) in the crypts. (1–2).

Simultaneously, IR transactivates *Wnt2b* via ROS-HIFs in IECs (3) and activates Wnt/ $\beta$ -catenin signaling in Tert+ cells (4), which results in the quiescence exit of Tert+ cells (5). Repopulation of Tert+ cells generates the progenitor and differentiated IECs (6). Finally, Tert+ cells re-enter into the quiescent state.